PHYSICAL REVIEW D **88,** 052019 (2013)

Measurement of $e^+e^- \to \omega\pi^0$, $K^*(892)\bar{K}$ and $K_2^*(1430)\bar{K}$ at $\sqrt{s}$ near 10.6 GeV

C. P. Shen,[2] C. Z. Yuan,[20] A. Sibidanov,[57] P. Wang,[20] K. Hayasaka,[40] X. L. Wang,[68] I. Adachi,[14] H. Aihara,[63] D. M. Asner,[49] T. Aushev,[24] A. M. Bakich,[57] A. Bala,[50] V. Bhardwaj,[41] B. Bhuyan,[17] A. Bondar,[4] G. Bonvicini,[69] A. Bozek,[45] M. Bračko,[34,25] T. E. Browder,[13] M.-C. Chang,[8] A. Chen,[42] B. G. Cheon,[12] R. Chistov,[24] I.-S. Cho,[71] K. Cho,[28] V. Chobanova,[35] S.-K. Choi,[11] Y. Choi,[56] D. Cinabro,[69] J. Dalseno,[35,59] Z. Doležal,[5] Z. Drásal,[5] A. Drutskoy,[24,37] D. Dutta,[17] S. Eidelman,[4] H. Farhat,[69] J. E. Fast,[49] T. Ferber,[7] A. Frey,[10] V. Gaur,[58] N. Gabyshev,[4] S. Ganguly,[69] R. Gillard,[69] Y. M. Goh,[12] B. Golob,[32,25] J. Haba,[14] H. Hayashii,[41] Y. Hoshi,[61] W.-S. Hou,[44] H. J. Hyun,[30] T. Iijima,[40,39] A. Ishikawa,[62] R. Itoh,[14] Y. Iwasaki,[14] T. Iwashita,[41] I. Jaegle,[13] T. Julius,[36] D. H. Kah,[30] J. H. Kang,[71] E. Kato,[62] T. Kawasaki,[47] C. Kiesling,[35] D. Y. Kim,[55] H. J. Kim,[30] H. O. Kim,[30] J. B. Kim,[29] J. H. Kim,[28] Y. J. Kim,[28] K. Kinoshita,[6] B. R. Ko,[29] P. Kodyš,[5] S. Korpar,[34,25] P. Križan,[32,25] P. Krokovny,[4] T. Kumita,[65] A. Kuzmin,[4] Y.-J. Kwon,[71] J. S. Lange,[9] S.-H. Lee,[29] Y. Li,[68] J. Libby,[18] C. Liu,[53] Y. Liu,[6] P. Lukin,[4] D. Matvienko,[4] H. Miyata,[47] R. Mizuk,[24,37] A. Moll,[35,59] T. Mori,[39] N. Muramatsu,[52] R. Mussa,[23] Y. Nagasaka,[15] M. Nakao,[14] Z. Natkaniec,[45] M. Nayak,[18] C. Ng,[63] S. Nishida,[14] O. Nitoh,[66] S. Ogawa,[60] S. Okuno,[26] Y. Onuki,[63] G. Pakhlova,[24] H. Park,[30] H. K. Park,[30] T. K. Pedlar,[33] R. Pestotnik,[25] M. Petrič,[25] L. E. Piilonen,[68] M. Ritter,[35] M. Röhrken,[27] A. Rostomyan,[7] S. Ryu,[54] H. Sahoo,[13] T. Saito,[62] Y. Sakai,[14] S. Sandilya,[58] L. Santelj,[25] T. Sanuki,[62] Y. Sato,[62] V. Savinov,[51] O. Schneider,[31] G. Schnell,[1,16] C. Schwanda,[21] D. Semmler,[9] K. Senyo,[70] M. Shapkin,[22] T.-A. Shibata,[64] J.-G. Shiu,[44] B. Shwartz,[4] F. Simon,[35,59] Y.-S. Sohn,[71] A. Sokolov,[22] E. Solovieva,[24] M. Starič,[25] M. Steder,[7] T. Sumiyoshi,[65] U. Tamponi,[23,67] K. Tanida,[54] G. Tatishvili,[49] Y. Teramoto,[48] M. Uchida,[64] S. Uehara,[14] T. Uglov,[24,38] Y. Unno,[12] S. Uno,[14] P. Urquijo,[3] S. E. Vahsen,[13] C. Van Hulse,[1] P. Vanhoefer,[35] G. Varner,[13] A. Vinokurova,[4] A. Vossen,[19] M. N. Wagner,[9] C. H. Wang,[43] Y. Watanabe,[26] K. M. Williams,[68] E. Won,[29] Y. Yamashita,[46] S. Yashchenko,[7] Y. Yook,[71] C. C. Zhang,[20] Z. P. Zhang,[53] and V. Zhilich[4]

(Belle Collaboration)

[1]*University of the Basque Country UPV/EHU, 48080 Bilbao*
[2]*Beihang University, Beijing 100191*
[3]*University of Bonn, 53115 Bonn*
[4]*Budker Institute of Nuclear Physics SB RAS and Novosibirsk State University, Novosibirsk 630090*
[5]*Faculty of Mathematics and Physics, Charles University, 121 16 Prague*
[6]*University of Cincinnati, Cincinnati, Ohio 45221*
[7]*Deutsches Elektronen-Synchrotron, 22607 Hamburg*
[8]*Department of Physics, Fu Jen Catholic University, Taipei 24205*
[9]*Justus-Liebig-Universität Gießen, 35392 Gießen*
[10]*II. Physikalisches Institut, Georg-August-Universität Göttingen, 37073 Göttingen*
[11]*Gyeongsang National University, Chinju 660-701*
[12]*Hanyang University, Seoul 133-791*
[13]*University of Hawaii, Honolulu, Hawaii 96822*
[14]*High Energy Accelerator Research Organization (KEK), Tsukuba 305-0801*
[15]*Hiroshima Institute of Technology, Hiroshima 731-5193*
[16]*Ikerbasque, 48011 Bilbao*
[17]*Indian Institute of Technology Guwahati, Assam 781039*
[18]*Indian Institute of Technology Madras, Chennai 600036*
[19]*Indiana University, Bloomington, Indiana 47408*
[20]*Institute of High Energy Physics, Chinese Academy of Sciences, Beijing 100049*
[21]*Institute of High Energy Physics, Vienna 1050*
[22]*Institute for High Energy Physics, Protvino 142281*
[23]*INFN-Sezione di Torino, 10125 Torino*
[24]*Institute for Theoretical and Experimental Physics, Moscow 117218*
[25]*J. Stefan Institute, 1000 Ljubljana*
[26]*Kanagawa University, Yokohama 221-8686*
[27]*Institut für Experimentelle Kernphysik, Karlsruher Institut für Technologie, 76131 Karlsruhe*
[28]*Korea Institute of Science and Technology Information, Daejeon 305-806*
[29]*Korea University, Seoul 136-713*
[30]*Kyungpook National University, Daegu 702-701*
[31]*École Polytechnique Fédérale de Lausanne (EPFL), Lausanne 1015*
[32]*Faculty of Mathematics and Physics, University of Ljubljana, 1000 Ljubljana*

[33]*Luther College, Decorah, Iowa 52101*
[34]*University of Maribor, 2000 Maribor*
[35]*Max-Planck-Institut für Physik, 80805 München*
[36]*School of Physics, University of Melbourne, Victoria 3010*
[37]*Moscow Physical Engineering Institute, Moscow 115409*
[38]*Moscow Institute of Physics and Technology, Moscow Region 141700*
[39]*Graduate School of Science, Nagoya University, Nagoya 464-8602*
[40]*Kobayashi-Maskawa Institute, Nagoya University, Nagoya 464-8602*
[41]*Nara Women's University, Nara 630-8506*
[42]*National Central University, Chung-li 32054*
[43]*National United University, Miao Li 36003*
[44]*Department of Physics, National Taiwan University, Taipei 10617*
[45]*H. Niewodniczanski Institute of Nuclear Physics, Krakow 31-342*
[46]*Nippon Dental University, Niigata 951-8580*
[47]*Niigata University, Niigata 950-2181*
[48]*Osaka City University, Osaka 558-8585*
[49]*Pacific Northwest National Laboratory, Richland, Washington 99352*
[50]*Panjab University, Chandigarh 160014*
[51]*University of Pittsburgh, Pittsburgh, Pennsylvania 15260*
[52]*Research Center for Electron Photon Science, Tohoku University, Sendai 980-8578*
[53]*University of Science and Technology of China, Hefei 230026*
[54]*Seoul National University, Seoul 151-742*
[55]*Soongsil University, Seoul 156-743*
[56]*Sungkyunkwan University, Suwon 440-746*
[57]*School of Physics, University of Sydney, New South Wales 2006*
[58]*Tata Institute of Fundamental Research, Mumbai 400005*
[59]*Excellence Cluster Universe, Technische Universität München, 85748 Garching*
[60]*Toho University, Funabashi 274-8510*
[61]*Tohoku Gakuin University, Tagajo 985-8537*
[62]*Tohoku University, Sendai 980-8578*
[63]*Department of Physics, University of Tokyo, Tokyo 113-0033*
[64]*Tokyo Institute of Technology, Tokyo 152-8550*
[65]*Tokyo Metropolitan University, Tokyo 192-0397*
[66]*Tokyo University of Agriculture and Technology, Tokyo 184-8588*
[67]*University of Torino, 10124 Torino*
[68]*CNP, Virginia Polytechnic Institute and State University, Blacksburg, Virginia 24061*
[69]*Wayne State University, Detroit, Michigan 48202*
[70]*Yamagata University, Yamagata 990-8560*
[71]*Yonsei University, Seoul 120-749*

(Received 2 September 2013; published 27 September 2013)

Using data samples of 89 fb^{-1}, 703 fb^{-1}, and 121 fb^{-1} collected with the Belle detector at the KEKB asymmetric-energy e^+e^- collider at center-of-mass energies 10.52 GeV, 10.58 GeV, and 10.876 GeV, respectively, we study the exclusive reactions $e^+e^- \to \omega\pi^0$, $K^*(892)\bar{K}$, and $K_2^*(1430)\bar{K}$. (Charge-conjugate modes are included implicitly.) Significant signals of $\omega\pi^0$, $K^*(892)^0\bar{K}^0$, and $K_2^*(1430)^-K^+$ are observed for the first time at these energies, and the energy dependencies of the cross sections are presented. On the other hand, no significant excesses for $K^*(892)^-K^+$ and $K_2^*(1430)^0\bar{K}^0$ are found, and we set limits on the cross section ratios $R_{\rm VP} = \frac{\sigma_B(e^+e^-\to K^*(892)^0\bar{K}^0)}{\sigma_B(e^+e^-\to K^*(892)^-K^+)} > 4.3$, 20.0, and 5.4, and $R_{\rm TP} = \frac{\sigma_B(e^+e^-\to K_2^*(1430)^0\bar{K}^0)}{\sigma_B(e^+e^-\to K_2^*(1430)^-K^+)} < 1.1$, 0.4, and 0.6, for center-of-mass energies of 10.52 GeV, 10.58 GeV, and 10.876 GeV, respectively, at the 90% C.L.

DOI: 10.1103/PhysRevD.88.052019 PACS numbers: 13.66.Bc, 13.25.Jx, 13.40.Gp, 14.40.Df

Large data samples collected at the B-factories provide an opportunity to explore rare two-meson production in e^+e^- annihilation, which allows us to investigate the energy dependence of various meson form factors and shed light on hadron structure and hence the strong interaction. These studies also supply information on the wave function of hadrons.

For a center-of-mass (CM) energy $\sqrt{s}$ much larger than resonance masses, one expects that the proportions of the cross sections of $\omega\pi^0$:$K^*(892)^0\bar{K}^0$:$K^*(892)^-K^+$

production equal 9:8:2 [1] if SU(3) flavor symmetry is exact. However, this relation was found to be violated severely at $\sqrt{s} = 3.67$ GeV and 3.773 GeV by the CLEO experiment [2], with the $\omega\pi^0$ cross sections smaller than those of the $K^*(892)^0\bar{K}^0$, and the ratio $R_{\rm VP} = \frac{\sigma_B(e^+e^-\to K^*(892)^0\bar{K}^0)}{\sigma_B(e^+e^-\to K^*(892)^-K^+)}$ greater than 9 and 33 at $\sqrt{s} =$ 3.67 GeV and 3.773 GeV, respectively, at the 90% confidence level (C.L.) [3].

By taking into account $SU(3)_{\rm f}$ symmetry breaking and the transverse momentum distribution of partons in the light cone wave functions of mesons, a perturbative quantum chromodynamics calculation [4] can reproduce most of the CLEO measurements with reasonable input parameters, and the corresponding cross sections at $\sqrt{s} =$ 10.58 GeV are predicted. The calculation predicts $R_{\rm VP} =$ 6.0, which is far below the CLEO lower limits and may indicate deficiencies in the model assumptions. The same calculation also predicts that the cross sections of $e^+e^- \to$ the vector pseudoscalar (VP) vary as $1/s^3$ rather than $1/s^2$ in Ref. [5] or $1/s^4$ in Refs. [6–8]; this can also be tested by combining the measurements from CLEO and the B-factories. At Belle, the cross sections of $e^+e^- \to \phi\eta$, $\phi\eta'$, $\rho\eta$, $\rho\eta'$ have been measured at $\sqrt{s} = 10.58$ GeV; however, no definite conclusion about the energy dependence of $e^+e^- \to VP$ can be drawn [9].

In the quark model, the tensor states $K_2^*(1430)$ have the same quark content as the vector states $K^*(892)$; thus, one may naively expect the same ratio between the neutral and charged $K_2^*(1430)\bar{K}$ production in e^+e^- annihilation as in the VP case, i.e., $R_{\rm TP} = \frac{\sigma_B(e^+e^-\to K_2^*(1430)^0\bar{K}^0)}{\sigma_B(e^+e^-\to K_2^*(1430)^-K^+)} = R_{\rm VP}$. This has never been tested.

In this paper, we report the cross sections of the exclusive reactions $e^+e^- \to \omega\pi^0$, $K^*(892)\bar{K}$, and $K_2^*(1430)\bar{K}$, based on data samples of 89 fb^{-1}, 703 fb^{-1}, and 121 fb^{-1} collected at $\sqrt{s} = 10.52$, 10.58 [$\Upsilon(4S)$ peak], and 10.876 GeV [$\Upsilon(5S)$ peak], respectively. The data were collected with the Belle detector [10] operating at the KEKB asymmetric-energy e^+e^- collider [11]. The final states are $\pi^+\pi^-\pi^0\pi^0$ and $K_S^0K^+\pi^-$, in which the K_S^0 is reconstructed from $\pi^+\pi^-$. The generator MCGPJ, developed according to the calculations in Ref. [12], is used to generate Monte Carlo (MC) events with the exact next-to-leading order radiative corrections applied to all the studied processes. Generic $e^+e^- \to u\bar{u}/d\bar{d}/s\bar{s}$ MC events, produced using PYTHIA [13], are used to check background contributions.

The Belle detector is described in detail elsewhere [10]. It is a large-solid-angle magnetic spectrometer that consists of a silicon vertex detector (SVD), a 50-layer central drift chamber (CDC), an array of aerogel threshold Cherenkov counters (ACC), a barrel-like arrangement of time-of-flight scintillation counters, and an electromagnetic calorimeter composed of CsI(Tl) crystals (ECL) located inside a superconducting solenoid coil that provides a 1.5 T magnetic field. An iron flux return located outside of the coil is instrumented to detect K_L^0 mesons and to identify muons (KLM).

For each charged track except those from K_S^0 decays, the impact parameters perpendicular to and along the beam direction with respect to the interaction point are required to be less than 0.5 cm and 4 cm, respectively, and the transverse momentum must exceed 0.1 GeV/c in the laboratory frame. Well-measured charged tracks are selected, and the numbers of such charged tracks are two for the $\pi^+\pi^-\pi^0\pi^0$ final state and four for the $K_S^0K^+\pi^-$ final state. For each charged track, we combine information from several detector subsystems to form a likelihood $\mathcal{L}_i$ for each particle species [14]. A track with $\mathcal{R}_K = \frac{\mathcal{L}_K}{\mathcal{L}_K+\mathcal{L}_\pi} > 0.6$ is identified as a kaon, while a track with $\mathcal{R}_K < 0.4$ is treated as a pion. With this selection, the kaon (pion) identification efficiency is about 85% (89%), while 6% (9%) of kaons (pions) are misidentified as pions (kaons). For electron identification, the likelihood ratio is defined as $\mathcal{R}_e = \frac{\mathcal{L}_e}{\mathcal{L}_e+\mathcal{L}_x}$, where $\mathcal{L}_e$ and $\mathcal{L}_x$ are the likelihoods for electron and nonelectron, respectively. These are determined using the ratio of the energy deposited in the ECL to the momentum measured in the SVD and CDC, the shower shape in the ECL, position matching between the charged track trajectory and the cluster position in the ECL, hit information from the ACC, and specific ionization (dE/dx) information in the CDC [15]. For muon identification, the likelihood ratio is defined as $\mathcal{R}_\mu = \frac{\mathcal{L}_\mu}{\mathcal{L}_\mu+\mathcal{L}_\pi+\mathcal{L}_K}$, where $\mathcal{L}_\mu$, $\mathcal{L}_\pi$, and $\mathcal{L}_K$ are the likelihoods for muon, pion, and kaon, respectively. These are based on track matching quality and penetration depth of associated hits in the KLM [16].

Except for the $\pi^+\pi^-$ pair from K_S^0 decay, all charged tracks are required to be positively identified as pions or kaons. The requirements $\mathcal{R}_\mu < 0.95$ and $\mathcal{R}_e < 0.95$ for the charged tracks remove 9.3% of the backgrounds for $K_S^0K^+\pi^-$ with negligible loss in efficiency.

For K_S^0 candidates decaying into $\pi^+\pi^-$ in the $K_S^0K^+\pi^-$ mode, we require that the invariant mass of the $\pi^+\pi^-$ pair lie within a ± 8 MeV/c^2 interval around the K_S^0 nominal mass, which contains around 95% of the signal according to MC simulation, and that the pair have a displaced vertex and flight direction consistent with a K_S^0 originating from the IP [17].

An energy cluster in the electromagnetic calorimeter is reconstructed as a photon if it does not match the extrapolated position of any charged track. A π^0 candidate is reconstructed from a pair of photons whose energies exceed 100 MeV in the laboratory frame. We perform a mass-constrained fit to the selected π^0 candidate and require $\chi^2 < 15$. To suppress background from the initial-state-radiative (ISR) process $e^+e^- \to \gamma_{\rm ISR}\omega \to \gamma_{\rm ISR}\pi^+\pi^-\pi^0$, the requirement of $|(E_1 - E_2)/(E_1 + E_2)| < 0.65$ is imposed for the primary π^0 of $e^+e^- \to \omega\pi^0$, where E_1 and

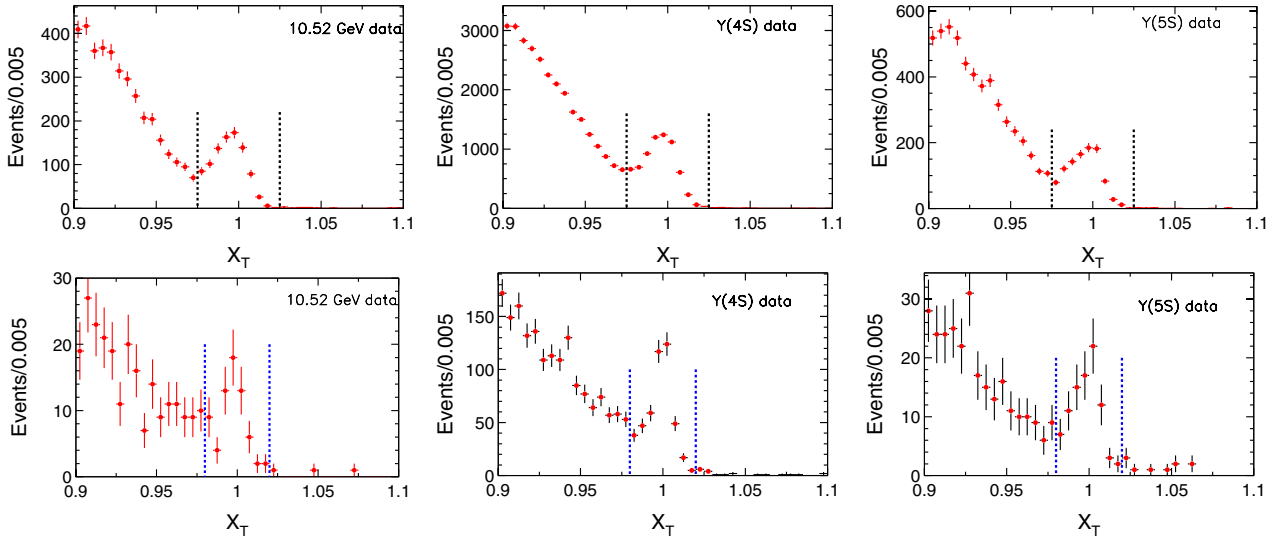

FIG. 1 (color online). The scaled total energy X_T distributions for the selected $e^+e^- \to \pi^+\pi^-\pi^0\pi^0$ (top row) and $K^0_S K^+\pi^-$ (bottom row) candidate events from the $\sqrt{s} = 10.52$ GeV, 10.58 GeV, and 10.876 GeV data samples. The signal region is between the dotted lines.

E_2 are the energies in the laboratory frame of the photons forming the higher-momentum π^0 candidate.

We define an energy conservation variable $X_T = \Sigma_h E_h/\sqrt{s}$, where E_h is the energy of the final-state particle h in the e^+e^- CM frame. For the signal candidates, X_T should be around 1. After the application of all the above selection requirements, Fig. 1 shows the X_T distributions for the final candidate events of $e^+e^- \to \pi^+\pi^-\pi^0\pi^0$ (top row) and $K^0_S K^+\pi^-$ (bottom row) from the $\sqrt{s} =$ 10.52 GeV, 10.58 GeV, and 10.876 GeV data samples, respectively. Clear $e^+e^- \to \pi^+\pi^-\pi^0\pi^0$ and $K^0_S K^+\pi^-$ signals are observed. We require $|X_T - 1| < 0.025$ for $\pi^+\pi^-\pi^0\pi^0$ and $|X_T - 1| < 0.02$ for $K^0_S K^+\pi^-$, as indicated by the dotted lines in Fig. 1.

The distributions of $M(\pi^+\pi^-\pi^0_l)$ versus $M(\pi^+\pi^-\pi^0_h)$ for the $\pi^+\pi^-\pi^0_h\pi^0_l$ final state and $M(K^0_S\pi^-)$ versus $M(K^+\pi^-)$ for the $K^0_S K^+\pi^-$ final state are shown in Fig. 2. Here, π^0_h and π^0_l represent the π^0 candidates with higher and lower momentum, respectively, in the laboratory system. According to MC-simulated $e^+e^- \to \omega\pi^0$ signal events, most of the π^0s ($> 97\%$) from ω decays have lower momentum and there is only one $\pi^+\pi^-\pi^0$ combination in the ω mass region. In the $K^0_S K^+\pi^-$ mode, we see clearly the intermediate states $K^*(892)\bar{K}$, $K^*_2(1430)\bar{K}$, and possibly $a_2(1320)\pi$.

For the selected events, Fig. 3 shows the $\pi^+\pi^-\pi^0$, $K^+\pi^-$, and $K^0_S\pi^-$ invariant mass distributions for the $\pi^+\pi^-\pi^0\pi^0$ and $K^0_S K^+\pi^-$ final states from the $\sqrt{s} =$ 10.52 GeV, 10.58 GeV, and 10.876 GeV data samples. For charge-conjugate modes the numbers of selected candidate events are consistent within 1 standard deviation. The dots with error bars are from data, and the light shaded histograms are from the normalized $e^+e^- \to u\bar{u}/d\bar{d}/s\bar{s}$ backgrounds. In the $\pi^+\pi^-\pi^0$ invariant mass distributions, the dark shaded histograms in the ω and ϕ mass regions are from the normalized $e^+e^- \to \gamma_{\rm ISR}\omega/\phi \to \gamma_{\rm ISR}\pi^+\pi^-\pi^0$ backgrounds. In the normalization, the expected ISR events are calculated with $N^{\rm prod} = \mathcal{L} \times \sigma^{\rm prod}$, where $\mathcal{L}$ is the integrated luminosity and $\sigma^{\rm prod}$ is the production cross section. The production cross sections are calculated to be $\sigma^{\rm prod}(e^+e^- \to \gamma_{\rm ISR}\omega) = 15.1$ pb, 14.9 pb, and 14.2 pb, and $\sigma^{\rm prod}(e^+e^- \to \gamma_{\rm ISR}\phi) = 25.4$ pb, 25.2 pb, and 23.9 pb, for $\sqrt{s} = 10.52$ GeV, 10.58 GeV, and 10.876 GeV, respectively [18]. ISR MC events of $e^+e^- \to \gamma_{\rm ISR}\omega/\phi \to \gamma_{\rm ISR}\pi^+\pi^-\pi^0$ are simulated using the PHOKHARA generator [19], which simulates the ISR process at the next-to-leading order accuracy. In the $K^+\pi^-$ and $K^0_S\pi^-$ invariant mass distributions, we observe clear $K^*(892)^0$ and $K^*_2(1430)^-$ signals, while almost no signals for $K^*_2(1430)^0$ and $K^*(892)^-$ can be seen.

We perform unbinned maximum likelihood fits to these mass distributions, as shown in Fig. 3. The signal shapes of ω, $K^*(892)$, and $K^*_2(1430)$ are obtained directly from MC simulated signal samples [20]. The combinatorial backgrounds are modeled by a second-order Chebyshev polynomial, and the additional normalized backgrounds from $e^+e^- \to \gamma_{\rm ISR}\omega/\phi \to \gamma_{\rm ISR}\pi^+\pi^-\pi^0$ are fixed in the $\pi^+\pi^-\pi^0$ mass spectrum fit. The fitted results are shown in Fig. 3 and listed in Table I.

The significances and the upper limits listed in Table I are obtained by evaluating the likelihood profile. To take into account the systematic uncertainty, we convolve the likelihood function with a Gaussian whose width equals the total systematic uncertainty. The significance is obtained by comparing the likelihood values at maximum

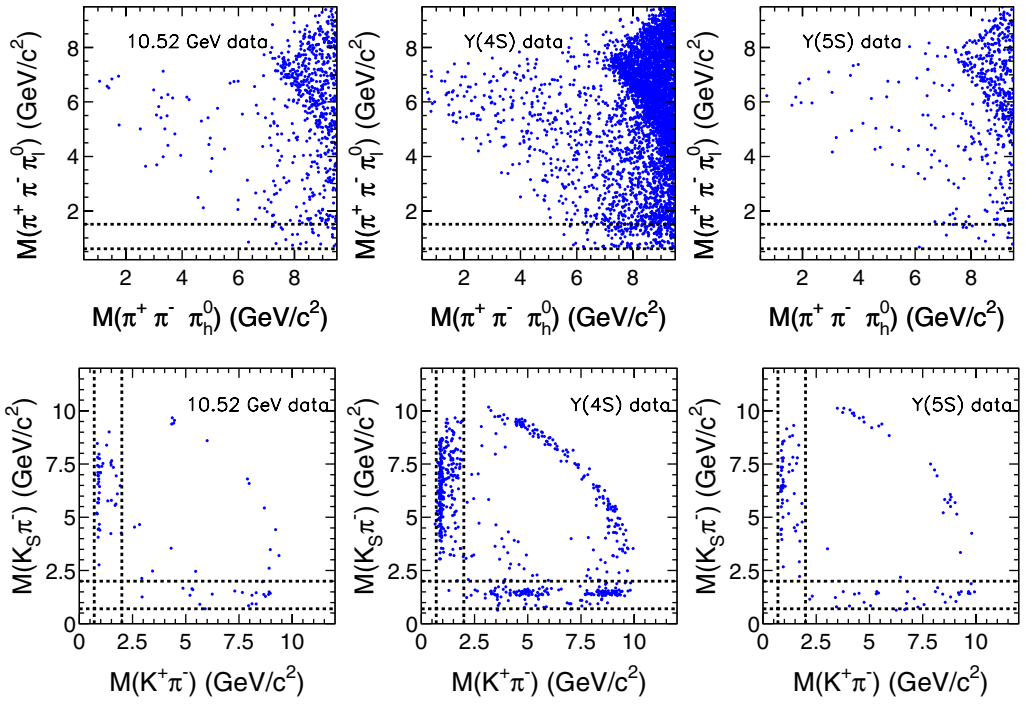

FIG. 2 (color online). Distributions of $M(\pi^+\pi^-\pi^0_l)$ versus $M(\pi^+\pi^-\pi^0_h)$ for the $\pi^+\pi^-\pi^0\pi^0$ (top row) and $M(K^0_S\pi^-)$ versus $M(K^+\pi^-)$ for the $K^0_S K^+\pi^-$ (bottom row) final states from the $\sqrt{s} = 10.52$ GeV, 10.58 GeV, and 10.876 GeV data samples. In the $\pi^+\pi^-\pi^0\pi^0$ panels, π^0_h and π^0_l represent the pions with higher and lower momentum in the laboratory system, respectively. The events between the dotted lines will be selected to search for ω, K^*, and K^*_2 signals.

and at zero signal yield using $\sqrt{-2\ln(\mathcal{L}_0/\mathcal{L}_{\max})}$. The upper limit $N^{\rm UL}_{\rm sig}$ on $N_{\rm sig}$ at 90% C.L. is obtained by integrating the likelihood function from zero to the bound that gives 90% of the total area.

The observed cross section is determined according to the formula $\sigma^{\rm obs} = \frac{N}{LB_{V/T}B_P\epsilon}$, where N is the signal yield, L is the integrated luminosity, $B_{\rm V/T}$ and $B_{\rm P}$ are the branching fractions of the corresponding decay channels of the vector/tensor and pseudoscalar mesons including secondary branching fractions to reconstructed final states, respectively, and ϵ is the corresponding detection efficiency. The Born cross section is written as $\sigma_B = \frac{\sigma^{\rm obs}|1-\Pi(s)|^2}{(1+\delta)}$, where $1+\delta$ is the radiative correction factor and $|1-\Pi(s)|^2$ is the vacuum polarization factor. The radiative correction factors $1+\delta$ are 0.89, 0.88, and 0.88 for $\omega\pi^0$, $K^*(892)\bar{K}$, and $K^*_2(1430)\bar{K}$, respectively, calculated with a limit on the energy of the radiated photon of 0.5 GeV [12]; the values of $|1-\Pi(s)|^2$ are 0.931, 0.930, and 0.929 [21] for $\sqrt{s} =$ 10.52 GeV, 10.58 GeV, and 10.876 GeV, respectively.

There are several sources of systematic uncertainties for the cross section measurements. The uncertainty in the tracking efficiency for tracks with angles and momenta characteristic of signal events is about 0.35% per track and is additive. The uncertainty due to particle identification efficiency is 1.7% with an efficiency correction factor of 0.98 for each pion and is 1.6% with an efficiency correction factor of 0.97 for each kaon. The uncertainty in selecting π^0 is estimated using a control sample of $\tau^- \to \pi^-\pi^0\nu_\tau$. We introduce a 2.2% systematic uncertainty with efficiency correction factors of 0.94 for a low momentum π^0 and 0.97 for a high momentum one. In the $K^0_S K^+\pi^-$ mode, the K^0_S reconstruction systematic uncertainty is estimated by comparing the ratio of the $D^+ \to K^0_S\pi^+$ and $D^+ \to K^-\pi^+\pi^+$ yields with the MC expectations; the difference between data and MC simulation is less than 4.9% [22]. Uncertainties on the branching fractions of the intermediate states are taken from the PDG listings [23]. According to MC simulation, the trigger efficiency is greater than 99% so the corresponding uncertainty is neglected. We estimate the systematic uncertainties associated with the fitting procedure by changing the shape of the background and the range of the fit and taking the differences in the fitted results, which are 1.0%–32% depending on the final state particles, as systematic uncertainties. The uncertainty due to limited MC statistics is at most 2.4%. The form factor dependence on s is assumed to be $\frac{1}{s}$ in the MCGPJ generator for the nominal results. The differences in the efficiency compared to the assumption of $\frac{1}{s^2}$ dependence for the form factor are taken as the systematic uncertainties due to the generator uncertainty, which are 1.5%, 0.9%, and 0.9% for the $\omega\pi^0$, $K^*(892)\bar{K}$, and $K^*_2(1430)\bar{K}$, respectively. We take 2% systematic uncertainty due to the uncertainty of the effect of soft and virtual photon emission in the generator [12]. The efficiency differences are 0.7% and 1.3% for $\omega\pi^0$ and $K^0_S K^+\pi^-$ final states, respectively,

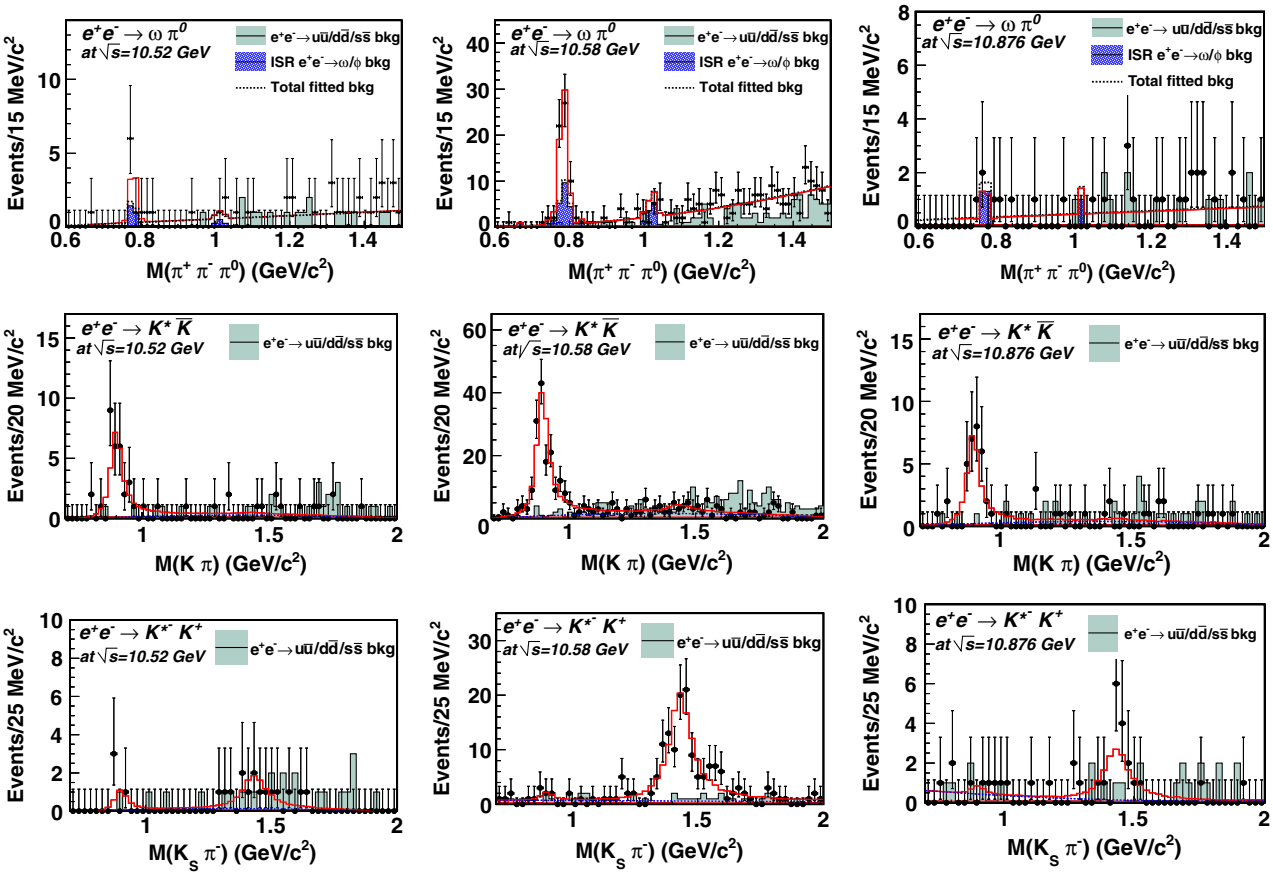

FIG. 3 (color online). The fits to the $\pi^+\pi^-\pi^0$ (top row), $K^+\pi^-$ (middle row), and $K^0_S\pi^-$ (bottom row) invariant mass distributions for the ω, $K^*(892)$, and $K^*_2(1430)$ meson candidates from $e^+e^- \to \pi^+\pi^-\pi^0\pi^0$ and $K^0_S K^+\pi^-$ events from the $\sqrt{s} = 10.52$ GeV, 10.58 GeV, and 10.876 GeV data samples. The solid lines show the results of the fits described in the text, the dotted curves show the total background estimates, the dark shaded histograms are from the normalized ISR backgrounds $e^+e^- \to \gamma_{\rm ISR}\omega/\phi \to \gamma_{\rm ISR}\pi^+\pi^-\pi^0$, and the light shaded histograms are from the normalized $e^+e^- \to u\bar{u}/d\bar{d}/s\bar{s}$ backgrounds. The dotted curves are not significantly seen in the signal regions due to low background level.

when including or excluding final state radiation [24]; these are included in the uncertainty of the generator. Finally, the total luminosity is determined using wide angle Bhabha events with 1.4% precision. Assuming that all of these systematic uncertainty sources are independent, the total systematic uncertainty is 6.8%–33%, depending on the final state, as shown in Table II.

Table I shows the results for the measured Born cross sections including the upper limits at 90% C.L. for the channels with a signal significance of less than 3σ. These are the first measurements of the cross sections and upper limits at CM energies 10.52 GeV, 10.58 GeV, and 10.876 GeV. The measured cross sections of $e^+e^- \to \omega\pi^0$ and $K^*(892)^0\bar{K}^0$ at $\sqrt{s} = 10.58$ GeV are consistent within errors with the theoretical predictions that range from $(4.1^{+0.5}_{-0.3})$ fb to $(5.2^{+0.4}_{-0.3})$ fb for $\omega\pi^0$ and from $(5.6^{+0.2}_{-0.4})$ fb to (7.1 ± 0.4) fb for $K^*(892)^0\bar{K}^0$ in Ref. [4]. In contrast, we do not observe a significant signal for $e^+e^- \to K^*(892)^-K^+$, and the upper limit of the cross section at 10.58 GeV is much lower than the prediction from the same calculation [4]. The measured cross section of $e^+e^- \to \omega\pi^0$ is much smaller than the calculated value of about 240 fb using the theoretical formulas in Ref. [5].

Figure 4 shows the cross sections measured in our experiment at $\sqrt{s} = 10.52$ GeV, 10.58 GeV, and 10.876 GeV for $e^+e^- \to \omega\pi^0$, $K^*(892)\bar{K}$, and $K^*_2(1430)\bar{K}$, where the uncertainties are the sum in quadrature of the statistical and systematic uncertainties. Since the signal significance is greater than 5σ for $e^+e^- \to K^*(892)^0\bar{K}^0$ at all energies and for $e^+e^- \to \omega\pi^0$ at $\sqrt{s} = 10.58$ GeV, we fit the $1/s^n$ dependence of the cross sections to our data and those from CLEO at $\sqrt{s} = 3.67$ GeV and 3.77 GeV [2]. The fit gives $n = 3.83 \pm 0.07$ and 3.75 ± 0.12 for $e^+e^- \to K^*(892)^0\bar{K}^0$ and $\omega\pi^0$ [25], respectively. These differ significantly from the $1/s^2$ [5] or $1/s^3$ [4] predictions and agree with $1/s^4$ [6–8] within 2.5σ. For other channels, no definite conclusion can be drawn from current results due to the large uncertainties.

TABLE I. Results for the Born cross sections, where $N_{\rm sig}$ is the number of fitted signal events, $N_{\rm sig}^{\rm UL}$ is the upper limit on the number of signal events, ϵ is the efficiency, Σ is the signal significance, σ_B is the Born cross section, and $\sigma_B^{\rm UL}$ is the upper limit on the Born cross section. All the upper limits are given at the 90% C.L. The first uncertainty in σ_B is statistical, and the second systematic.

Channel	$\sqrt{s}$ [GeV]	$N_{\rm sig}$	$N_{\rm sig}^{\rm UL}$	ϵ [%]	Σ (σ)	σ_B [fb]	$\sigma_B^{\rm UL}$ [fb]
$\omega\pi^0$	10.52	$4.1^{+3.3}_{-2.6}$	9.9	1.25	1.6	$4.53^{+3.64}_{-2.88} \pm 0.50$	11
	10.58	$38.8^{+8.3}_{-7.6}$	...	1.10	6.7	$6.01^{+1.29}_{-1.18} \pm 0.57$	...
	10.876	$-0.7^{+2.9}_{-2.1}$	7.0	1.07	...	$-0.68^{+2.71}_{-1.97} \pm 0.20$	6.5
$K^*(892)^0\bar{K}^0$	10.52	$34.6^{+6.9}_{-6.1}$	...	16.49	7.4	$10.77^{+2.15}_{-1.90} \pm 0.77$	...
	10.58	187 ± 17	...	16.30	>10	$7.48 \pm 0.67 \pm 0.51$	...
	10.876	$34.6^{+7.5}_{-6.7}$	...	17.25	7.2	$7.58^{+1.64}_{-1.47} \pm 0.63$	...
$K^*(892)^-K^+$	10.52	$4.6^{+3.6}_{-2.7}$	9.3	20.40	1.4	$1.14^{+0.90}_{-0.67} \pm 0.15$	2.3
	10.58	$5.9^{+4.7}_{-3.8}$	14	21.03	1.5	$0.18^{+0.14}_{-0.12} \pm 0.02$	0.4
	10.876	$1.6^{+3.9}_{-3.0}$	8.5	21.29	0.3	$0.28^{+0.68}_{-0.52} \pm 0.10$	1.5
$K_2^*(1430)^0\bar{K}^0$	10.52	$1.3^{+4.3}_{-3.9}$	6.8	17.63	0.3	$0.76^{+2.53}_{-2.26} \pm 0.14$	4.0
	10.58	21^{+11}_{-10}	40	16.71	2.1	$1.65^{+0.86}_{-0.78} \pm 0.27$	3.1
	10.876	$1.0^{+4.5}_{-3.7}$	8.9	19.02	0.2	$0.38^{+1.79}_{-1.47} \pm 0.07$	3.5
$K_2^*(1430)^-K^+$	10.52	$12.0^{+6.2}_{-5.8}$	21	20.36	2.1	$6.06^{+3.13}_{-2.93} \pm 1.34$	11
	10.58	129 ± 15	...	20.17	>10	$8.36 \pm 0.95 \pm 0.62$	...
	10.876	$17.6^{+5.3}_{-4.6}$	...	21.50	4.5	$6.20^{+1.86}_{-1.63} \pm 0.64$	...

In all the above discussions, we neglect possible small contributions from $\Upsilon(4S)$ and $\Upsilon(5S)$ resonance decays in the measured Born cross sections at $\sqrt{s} = 10.58$ GeV and 10.876 GeV. Since the signal significance exceeds 5σ for the $K^*(892)^0\bar{K}^0$ mode at the continuum energy $\sqrt{s} = 10.52$ GeV, we can estimate the continuum contributions at $\sqrt{s} = 10.58$ GeV and 10.876 GeV under the assumption that the continuum cross section varies as $1/s^4$. After subtracting the continuum contributions, the net contribution to the cross sections from $\Upsilon(4S)$ and $\Upsilon(5S)$ decays is determined to be (-4.5 ± 3.7) fb and (-0.8 ± 3.1) fb, respectively. Here, the errors are statistical and systematic combined, and the common systematic errors are counted once. The efficiencies and the radiative correction factors are reevaluated assuming the events are from $\Upsilon(4S)$ or $\Upsilon(5S)$ decays, and possible interference between the continuum and resonant amplitudes is neglected. The total production cross sections of $\Upsilon(4S)$ and $\Upsilon(5S)$ are (2.06 ± 0.11) nb and (0.70 ± 0.39) nb, calculated with the world average values of their masses and partial widths to electron pairs [23]. By generating toy MC samples, assuming both the $K^*(892)^0\bar{K}^0$ and the total production cross sections follow Gaussian distributions (the mean values and standard deviations being set to the central values and corresponding errors of the cross sections, respectively), we obtain the distribution of the ratio of the two cross sections, from which the decay branching fraction upper limits $\mathcal{B}(\Upsilon(4S) \to K^*(892)^0\bar{K}^0) < 2.0 \times 10^{-6}$ and $\mathcal{B}(\Upsilon(5S) \to K^*(892)^0\bar{K}^0) < 1.0 \times 10^{-5}$ at 90% C.L. are determined. These results indicate that the contributions from $\Upsilon(4S)$ and $\Upsilon(5S)$ resonance decays are insignificant.

TABLE II. Relative systematic uncertainties (%) on the cross section. For the fit uncertainty and the total systematic uncertainty, the three values separated by slashes are for the CM energies 10.52 GeV, 10.58 GeV, and 10.876 GeV, respectively.

Source	$\omega\pi^0$	$K^*(892)^0\bar{K}^0$	$K^*(892)^-K^+$	$K_2^*(1430)^0\bar{K}^0$	$K_2^*(1430)^-K^+$
Tracking	0.7	0.7	0.7	0.7	0.7
Particle identification	3.4	3.3	3.3	3.3	3.3
π^0 selection	4.4	...	...	...	...
K_S^0 selection	...	4.9	4.9	4.9	4.9
Branching fractions	0.8	0.1	0.1	2.4	2.4
Fit uncertainty	8.8/6.6/28	2.4/1.0/4.9	11/8.2/32	16/14/15	21/2.2/7.4
MC statistics	2.4	0.8	0.8	0.7	0.7
Generator	2.6	2.6	2.6	2.6	2.6
Luminosity	1.4	1.4	1.4	1.4	1.4
Sum in quadrature	11/9.5/29	7.1/6.8/8.3	13/11/33	18/16/17	22/7.4/11

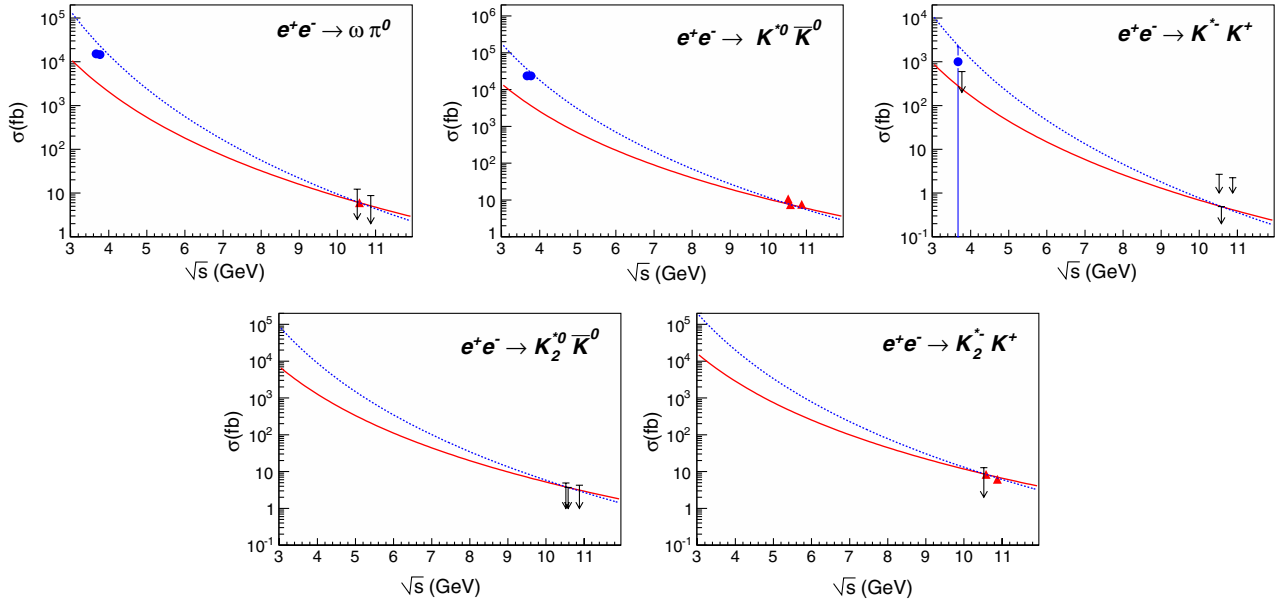

FIG. 4 (color online). The cross sections for $e^+e^- \to \omega\pi^0$, $K^*(892)\bar{K}$, and $K_2^*(1430)\bar{K}$. The data at $\sqrt{s} = 10.52$ GeV, 10.58 GeV, and 10.876 GeV are from our measurements. The data at $\sqrt{s} = 3.67$ GeV and 3.77 GeV, where shown, are from CLEO measurements [2]. Here, the uncertainties are the sum of the statistical and systematic uncertainties in quadrature. Upper limits are shown by the arrows. The solid line corresponds to a $1/s^3$ dependence and the dashed line to a $1/s^4$ dependence; the curves pass through the measured cross section at $\sqrt{s} = 10.58$ GeV.

Based on the likelihood curves of the cross section measurements, in which the relevant systematic uncertainties are convolved, we obtain

$$R_{\rm VP} = \frac{\sigma_B(e^+e^- \to K^*(892)^0\bar{K}^0)}{\sigma_B(e^+e^- \to K^*(892)^-K^+)} > 4.3, \quad 20.0, \quad 5.4,$$

and

$$R_{\rm TP} = \frac{\sigma_B(e^+e^- \to K_2^*(1430)^0\bar{K}^0)}{\sigma_B(e^+e^- \to K_2^*(1430)^-K^+)} < 1.1, \quad 0.4, \quad 0.6,$$

for $\sqrt{s} = 10.52$ GeV, 10.58 GeV, and 10.876 GeV, respectively, at the 90% C.L. Assuming that the cross section dependence on s is $1/s^n$ ($n = 3.83$) from our measurement of $K^*(892)^0\bar{K}^0$ and that this assumption is applicable to all the final states, we obtain the weighted average of the cross sections at a luminosity-weighted energy point of 10.61 GeV, which are $(7.86^{+0.72}_{-0.71})$ fb, $(0.54^{+0.13}_{-0.12})$ fb, $(1.36^{+0.77}_{-0.69})$ fb, and $(7.81^{+0.96}_{-0.93})$ fb for $K^*(892)^0\bar{K}^0$, $K^*(892)^-K^+$, $K_2^*(1430)^0\bar{K}^0$, and $K_2^*(1430)^-K^+$, respectively. For $K_2^*(1430)^0\bar{K}^0$ and $K_2^*(1430)^-K^+$, based on the above weighted average of the cross sections at $\sqrt{s} = 10.61$ GeV and the assumption of the cross section dependence on s, we obtain $(3.8^{+2.1}_{-1.9})$ pb and $(21.6^{+2.7}_{-2.6})$ pb at $\sqrt{s} = 3.77$ GeV. The uncertainties are the sum in quadrature of the statistical and systematic uncertainties. We obtain the averaged ratios as $\bar{R}_{\rm VP} > 10.9$ and $\bar{R}_{\rm TP} < 0.3$ at the 90% C.L. Here, for the calculated ratios, the common systematic uncertainties cancel.

For $K^*(892)\bar{K}$, the ratio of the cross sections of $K^*(892)^0\bar{K}^0$ and $K^*(892)^-K^+$ at $\sqrt{s} = 10.58$ GeV is much larger than the predictions from exact or broken SU(3) symmetry models. Conversely, for $K_2^*(1430)\bar{K}$, the ratio of the cross sections of $K_2^*(1430)^0\bar{K}^0$ and $K_2^*(1430)^-K^+$ is much smaller than the prediction from the SU(3) symmetry or with the SU(3) symmetry breaking effects considered.

In a naive quark model developed to explain the transition-rate difference between $K_2^*(1430)^0 \to K^0\gamma$ and $K_2^*(1430)^+ \to K^+\gamma$ [27], one obtains $R_{\rm TP} \ll 1$ by assuming the model can be extended to a timelike virtual-photon case; this extrapolation is justified since the same model predicted the ratio of $\frac{\Gamma(K_2^*(1430)^0\to K^0\gamma)}{\Gamma(K_2^*(1430)^+\to K^+\gamma)} = 0.054$, in rough agreement with the experimental measurement [27]. In the same model, however, the radiative transitions between $K^*(892)$ and K were also calculated, and a ratio $\frac{\Gamma(K^*(892)^0\to K^0\gamma)}{\Gamma(K^*(892)^+\to K^+\gamma)} = 1.7$ was obtained, which is very different from the measurements of $R_{\rm VP}$ from both this and CLEO [2] experiments.

In summary, we have measured for the first time the cross sections for the reactions $e^+e^- \to \omega\pi^0$, $K^*(892)\bar{K}$, and $K_2^*(1430)\bar{K}$ at CM energies between 10 and 11 GeV. The results are summarized in Table I. Significant signals of $\omega\pi^0$, $K^*(892)^0\bar{K}^0$, and $K_2^*(1430)^-K^+$ are observed, while no significant excess for $K^*(892)^-K^+$ and $K_2^*(1430)^0\bar{K}^0$ is found. The ratios $R_{\rm VP}$ and $R_{\rm TP}$ at the 90% C.L. are given.

We thank the KEKB group for excellent operation of the accelerator; the KEK cryogenics group for efficient solenoid operations; and the KEK computer group, the NII, and PNNL/EMSL for valuable computing and SINET4 network support. We acknowledge support from MEXT, JSPS, and Nagoya's TLPRC (Japan); ARC and DIISR (Australia); FWF (Austria); NSFC (China); MSMT (Czechia); CZF, DFG, and VS (Germany); DST (India); INFN (Italy); MEST, NRF, GSDC of KISTI, and WCU (Korea); MNiSW and NCN (Poland); MES and RFAAE (Russia); ARRS (Slovenia); IKERBASQUE and UPV/EHU (Spain); SNSF (Switzerland); NSC and MOE (Taiwan); and DOE and NSF (USA). This work is supported partly by the Fundamental Research Funds for the Central Universities of China (303236).

[1] Charge-conjugate decays are implicitly assumed throughout the paper.
[2] N. E. Adam *et al.* (CLEO Collaboration), Phys. Rev. Lett. **94**, 012005 (2005); G. S. Adams *et al.* (CLEO Collaboration), Phys. Rev. D **73**, 012002 (2006).
[3] This is our own calculation based on the values of the cross sections from Ref. [2].
[4] C. D. Lü, W. Wang, and Y. M. Wang, Phys. Rev. D **75**, 094020 (2007).
[5] J.-M. Gérard and G. López Castro, Phys. Lett. B **425**, 365 (1998).
[6] V. L. Chernyak and A. R. Zhitnitsky, JETP Lett. **25**, 510 (1977); G. P. Lepage and S. J. Brodsky, Phys. Rev. D **22**, 2157 (1980); S. J. Brodsky and G. P. Lepage, Phys. Rev. D **24**, 2848 (1981).
[7] V. Chernyak, arXiv:hep-ph/9906387; V. L. Chernyak and A. R. Zhitnitsky, Phys. Rep. **112**, 173 (1984).
[8] V. V. Braguta, A. K. Likhoded, and A. V. Luchinsky, Phys. Rev. D **78**, 074032 (2008).
[9] K. Belous *et al.* (Belle Collaboration), Phys. Lett. B **681**, 400 (2009).
[10] A. Abashian *et al.* (Belle Collaboration), Nucl. Instrum. Methods Phys. Res., Sect. A **479**, 117 (2002); also see detector section in J. Brodzicka *et al.*, Prog. Theor. Exp. Phys. 04D001 (2012).
[11] S. Kurokawa and E. Kikutani, Nucl. Instrum. Methods Phys. Res., Sect. A **499**, 1 (2003), and other papers included in this volume; T. Abe *et al.*, Prog. Theor. Exp. Phys. 03A001 (2013), and following articles up to 03A011.
[12] A. B. Arbuzov, E. A. Kuraev, G. V. Fedotovich, N. P. Merenkov, V. D. Rushai, and L. Trentadue, J. High Energy Phys. 10 (1997) 001; A. B. Arbuzov, E. A. Kuraev, V. A. Astakhov, G. V. Fedotovich, A. V. Fedorov, and N. P. Merenkov, *ibid.* 10 (1997) 006; A. B. Arbuzov, G. V. Fedotovich, F. V. Ignatov, E. A. Kuraev, and A. L. Sibidanov, Eur. Phys. J. C **46**, 689 (2006); S. Actis *et al.*, Eur. Phys. J. C **66**, 585 (2010).
[13] T. Sjöstrand, S. Mrenna, and P. Skands, J. High Energy Phys. 05 (2006) 026.
[14] E. Nakano, Nucl. Instrum. Methods Phys. Res., Sect. A **494**, 402 (2002).
[15] K. Hanagaki, H. Kakuno, H. Ikeda, T. Iijima, and T. Tsukamoto, Nucl. Instrum. Methods Phys. Res., Sect. A **485**, 490 (2002).
[16] A. Abashian *et al.*, Nucl. Instrum. Methods Phys. Res., Sect. A **491**, 69 (2002).
[17] F. Fang, Ph.D. thesis, University of Hawaii, 2003 (http://belle.kek.jp/bdocs/theses.html).
[18] N. Brambilla *et al.*, arXiv:hep-ph/0412158.
[19] G. Rodrigo, H. Czyż, J. H. Kühn, and M. Szopa, Eur. Phys. J. C **24**, 71 (2002).
[20] The $\pi^+\pi^-\pi^0$ mass resolutions in data and MC simulation are checked using the control sample of $e^+e^- \to \gamma_{\rm ISR}\omega \to \gamma_{\rm ISR}\pi^+\pi^-\pi^0$ and are found to be consistent.
[21] F. Jegerlehner, Z. Phys. C **32**, 195 (1986); H. Burkhardt, F. Jegerlehner, G. Penso, and C. Verzegnassi, Z. Phys. C **43**, 497 (1989); S. Eidelman and F. Jegerlehner, Z. Phys. C **67**, 585 (1995); F. Jegerlehner, Nucl. Phys. B, Proc. Suppl. **131**, 213 (2004); **162**, 22 (2006); **181–182**, 135 (2008).
[22] S.-W. Lin *et al.* (Belle Collaboration), Phys. Rev. Lett. **99**, 121601 (2007).
[23] J. Beringer *et al.* (Particle Data Group), Phys. Rev. D **86**, 010001 (2012), and 2013 partial update for the 2014 edition.
[24] E. Richter-Was, Phys. Lett. B **303**, 163 (1993).
[25] With this energy dependence, we can calculate the branching fraction of $\Upsilon(1S) \to \omega\pi^0$ according to $\frac{\mathcal{B}(\Upsilon(1S)\to\omega\pi^0)}{\mathcal{B}(\Upsilon(1S)\to\mu^+\mu^-)} = \frac{\sigma_B(e^+e^-\to\omega\pi^0)}{\sigma_B(e^+e^-\to\mu^+\mu^-)}$ assuming $\Upsilon(1S)$ decays into $\omega\pi^0$ via one-photon annihilation only. Here the cross sections are at $\sqrt{s} = m_{\Upsilon(1S)}$, with $m_{\Upsilon(1S)}$ being the nominal mass of the $\Upsilon(1S)$. We obtain $\mathcal{B}(\Upsilon(1S) \to \omega\pi^0) = (3.56^{+0.83}_{-0.78}) \times 10^{-7}$, which is 1 order of magnitude lower than the upper limit determined in Ref. [26] and about 2 orders of magnitude lower than the prediction in Ref. [5].
[26] C. P. Shen *et al.* (Belle Collaboration), Phys. Rev. D **88**, 011102 (2013).
[27] D. Carlsmith *et al.*, Phys. Rev. D **36**, 3502 (1987).